



Wang, H., Celik, A., Zang, B., Rezgui, D., & Azarpeyvand, M. (2019). An Experimental Investigation of Propeller Noise in Forward Flow. In *25th AIAA/CEAS Aeroacoustics Conference* [AIAA 2019-2620] Delft, The Netherlands: American Institute of Aeronautics and Astronautics Inc. (AIAA). <https://doi.org/10.2514/6.2019-2620>

Peer reviewed version

Link to published version (if available):  
[10.2514/6.2019-2620](https://doi.org/10.2514/6.2019-2620)

[Link to publication record in Explore Bristol Research](#)  
PDF-document

This is the author accepted manuscript (AAM). The final published version (version of record) is available online via AIAA at <https://arc.aiaa.org/doi/10.2514/6.2019-2620> . Please refer to any applicable terms of use of the publisher.

## University of Bristol - Explore Bristol Research

### General rights

This document is made available in accordance with publisher policies. Please cite only the published version using the reference above. Full terms of use are available:  
<http://www.bristol.ac.uk/pure/about/ebr-terms>

# An experimental investigation of propeller noise in forward flow

Haifei Wang<sup>1,2</sup>, B. Zang<sup>2</sup>, Alper Celik<sup>2</sup>, Djamel Rezgui<sup>2</sup>, Mahdi Azarpeyvand<sup>2</sup>

1. Yangzhou University, College of Mechanical Engineering, Yangzhou, 225127, P. R. China,

2. University of Bristol, Queen's Building, Bristol, BS8 1TR, United Kingdom

The present experimental study characterizes the noise generated by small propellers in static and in-forward-flight conditions. A set of experiments were conducted in the aeroacoustic wind tunnel of the University of Bristol, in which both the aeroacoustic noise and aerodynamic loads were measured simultaneously for the selected propeller blades, having similar propeller diameter (11 inches) and pitch (from 4 to 10 inches) to those commonly used in small unmanned aerial vehicles. The tests were performed with incoming flow velocities from 0 m/s to 20 m/s for a range of propeller rotational speeds from 2500 RPM to 5500 RPM. The results show that the characteristics of noise consist of an overall broadband hump overlaid with distinct narrow peaks, corresponding to the fundamental blade passing frequency and its harmonics, regardless of the flow velocities. Moreover, the synchronous aerodynamic and noise measurements confirm that as the flow velocity increases, the reduction on aerodynamic loads leads to reduction in the overall noise generation by the propeller, indicating a direct correlation between aerodynamic load and propeller noise. This is further corroborated when comparing across propellers with different pitch values. The propeller with the highest pitch of 10 inches consistently produces louder noise than the other propellers. The results shed more lights on the choice of propellers pitch angles and their operational profile with respect to the propeller noise generation.

## Nomenclature

x	=	coordinate axis in plane with propeller rotation
y	=	coordinate axis in plane with propeller rotation
z	=	coordinate axis out of plane with propeller rotation
r	=	blade radial position [mm]
RPM	=	revolutions per minute
R	=	radius of propeller [mm]
$\beta$	=	blade pitch angle [°]
$\theta$	=	angle between microphone and plane of propeller rotation [°]
n	=	order of the blade pass frequency harmonics
BPF	=	blade passing frequency [Hz]
SPL	=	sound pressure level [dB]
U	=	Uniform inflow velocity [m/s]
D	=	Propeller diameter [m]

---

Haifei Wang, Lecturer in Mechanical Engineering, Yangzhou university, and research associate in Aeroacoustics, Department of Mechanical Engineering, University of Bristol, hw17162@bristol.ac.uk;

Bin Zang, Research Associate, Department of Aerospace Engineering, University of Bristol, nick.zang@bristol.ac.uk;

Alper Celik, Research Associate, Department of Mechanical Engineering, University of Bristol, alper.celik@bristol.ac.uk;

Djamel Rezgui, Lecturer in Aerospace Engineering, Department of Aerospace Engineering, University of Bristol, Djamel.Rezgui@bristol.ac.uk;

Mahdi Azarpeyvand, Reader in Aeroacoustics, Department of Mechanical Engineering, University of Bristol, m.azarpeyvand@bristol.ac.uk.

$\Omega$	=	Rotational speed [RPM]
$F_s$	=	Sample frequency [Hz]
$T_s$	=	Sample time [s]
$\nu$	=	kinematic viscosity of air at 20°C (m <sup>2</sup> /s)

## I. Introduction

UNMANNED aerial vehicles (UAVs) have become increasingly popular in recent years due to their versatility. Not only do they provide a stable and manageable airborne platform, they are designed at various sizes and configurations to fulfill the different mission requirements in terms of payload, maneuverability, range and endurance. On the other hand, the noise generated by UAVs has become a significant issue of concern. In military operations, noise reduction equates to better survivability and surveillance<sup>1</sup> whereas in civilian deployment, noise reduction alleviates health problems associated with prolonged exposure to elevated level of noise<sup>2</sup>. While noise reduction is achievable through various means, it is crucial that these methods do not affect significantly the aerodynamic performance and handling of the vehicles. As a result, in order to propose innovative solutions to noise reduction in UAVs, it is imperative to understand the aeroacoustic characteristics and noise generation mechanisms of the system.

Propeller self-noise is one of the major contributions in the noise generated from the UAV platforms. It is primarily generated by interactions between the flow and the trailing edge and tip of a propeller<sup>3,4</sup>. The noise signatures of the propeller self-noise consist of a broadband noise produced through the interactions of turbulent flow, caused by boundary layer instability, with the trailing edge and several tonal noises related to the vortices shed by the propeller tips at multiples of the blade passing frequency. In addition, blade-vortex interactions (BVI) also generate a noticeable amount of noise due to pressure fluctuations on a blade induced from the previously generated tip vortices<sup>5</sup>.

Indeed, propeller performance at low Reynolds numbers has become increasingly important in the design and performance prediction of the UAVs. However, study on propellers at low Reynolds numbers has been rather limited. Bailey<sup>6</sup> documented experimental tests on seven wooden Top Flite™ model-airplane propellers ranging in diameter from 9 to 14 inch. It was reported that those results showed propeller efficiencies of approximately 7.5% to 15% lower than the larger 36-in diameter propellers having similar pitch-to-diameter ratios, as tested by Durand<sup>7</sup>. Similar degradation in performance was later measured by Bass<sup>8</sup> for propellers larger than 24-in diameter, and by Asson and Dunn<sup>9</sup>, who obtained measurements on two wooden 14-in diameter Zinger brand model airplane propellers. During the same period, when the present study was carried out, Merchant and Miller<sup>10</sup> conducted a comprehensive study on as many as 30 model airplane propellers ranging in diameter from 6 to 22 in and created a database for optimize propellers, but only a subset of the measurements on seven propellers have been reported from that effort<sup>11,12</sup>. More recently, Ol, et al.<sup>13</sup> carried out measurements on many propellers UAVs and made detailed analyses and comparisons to reveal low Reynolds number effects, especially for propellers of small diameter, large blade taper ratio and operation at low advance ratio. It was found that predictions and accurate capture of Reynolds number effects were very sensitive to propeller twist and chord distributions. A total number of 79 propellers were tested and nearly all within the 9 to 11 in diameter range. Thrust and torque were measured over a range of propeller advance ratios for discrete propeller speeds (RPM's) at low Reynolds number. The results showed significant Reynolds number effects with degradation in performance with lower RPM's. Also, over a ranger of propellers, the propeller efficiency varied greatly from a peak near 0.65 down to near 0.28 for an exceptionally poor propeller. Moreover, John and Michael, in their study on propeller performance, determined the static thrust over a range of propeller speeds from nominally 1500 to 7500 RPM depending on the propeller diameter<sup>14</sup>, and observed that propeller efficiencies varied greatly from 0.28 to 0.65, which indicated that the proper selection of propellers the proper propeller selection had a great effect on aircraft performance. Cambray et al.<sup>15</sup> conducted experiments on near-field and far-field noise of UAV with different pitch angles and blades with serrated trailing edges. Results show that increasing of pitch angle leads to greater broadband and tonal noise. Furthermore, Nikolas<sup>16</sup> conducted performance and acoustic measurements of an isolated unmanned aircraft system (UAS) rotor in hover conditions and compared favorably with previously measured data in an anechoic chamber and blade element-based acoustic predictions. Static thrust measurements made in the Low Speed Aeroacoustic Wind Tunnel (LSAWT) are in excellent agreement with measurement made in the Structural Acoustics Loads and Transmission (SALT) anechoic chamber on the

same rotor. Acoustic directivity measurements identified deviation at characteristic frequencies and BPF is agree with prediction for frequencies above the estimated cut-on frequency.

In order to understand the noise generation mechanism for development of more robust noise control techniques, such as serrations [18], porous material [19], the present experimental work is performed with the objective to complement the previous studies by Cambray et al. as well as to shed more light upon the noise generation mechanism of small diameter propeller blades, particularly, when these blades are subjected to a steady incoming flow (i.e. in-forward-flight conditions). A series of measurements has been carried out to observe the variations of broadband and tonal noises with different propeller loads, which are in-turn controlled carefully using a combination of different propeller pitches, rotational speeds as well as the incoming flow velocities.

## II. Methodology

The experiments were performed in the University of Bristol Aeroacoustic facility, which is a closed-circuit, open-jet anechoic wind tunnel. The anechoic chamber has a cut-off frequency of 160 Hz with dimensions of 6.7m  $\times$  4m  $\times$  3m. The nozzle of the wind tunnel has an area of 0.5m  $\times$  0.775m (width  $\times$  height) which allows a steady-operation from 5m/s to 40m/s. The present experiments were conducted with free stream velocities varying from 5m/s to 20m/s, which corresponds to Reynolds numbers from 100,000 to 400,000 based on propeller diameter (i.e.  $Re_D = UD/\nu$ ). The anechoic wind tunnel is designed to provide a ‘silent’ air flow system with sufficiently low background noise for far-field noise measurements, with a far-field microphone array consisting of 23 1/4" GRAS 40PL microphones spanning from 45° to 130° at 5° interval. The microphone array is installed on a polar arc, located 1.65m top of the working section along the centerline of the nozzle. In order to simulate the in-flight conditions under ordinary UAV operational profile, the test rig was positioned in the middle of the open jet nozzle, approximately 600mm away from the nozzle exit, as shown in Figure 1, as such, to prevent undesirable acoustic reflections from the nozzle lip as well as to remain within the jet potential core for flow uniformity<sup>17</sup>. Readers are advised to refer to Mayer et al.<sup>17</sup> for details on the flow characteristics of the anechoic wind tunnel.

Figure 2 presents the images of the test rig used for this experimental study. The propeller rig was designed to allow for testing various propeller blades. The rig is composed of a small brushless motor, a 3D printed nacelle, a load cell, and supporting structures. Electronic speed control (ESC) is used to control and regulate the speed of brushless motor. The thermal limitations of the motor and ESC were considered for the desired operational rotational speed range. A NovaTech F310 axial force and torque transducer was mounted directly behind the motor to measure the aerodynamic loads from the propellers in static and in-flight conditions, at a sampling rate of 1000Hz and an accuracy of  $\pm 0.5\%$ . The data is collected using National instrument 9234 card and the data is collected via RCbenchmark software. The supporting structures are housed in a hub with an aerodynamic shape to avoid any noise interferences from the individual components. The propeller blades and its mounting structures are securely connected to the floor to reduce any mechanical vibrations.

A schematic of the far-field noise measurement experimental set-up is demonstrated in Figure 3. All noise measurements are collected with National Instrument PXI4499 data acquisition cards at a sampling frequency of  $2^{16}$  Hz and a sampling duration of 16s to ensure data convergence. The collected data were then subjected to standard *pwelch* function coupled with Hanning window and a 90% overlap to compute power spectral density, PSD (dB/Hz).

To study the effect of propeller pitch angle, a series of constant-pitch propellers with identical diameter and varying pitch values were used. Seven commercially available APC model aircraft propellers were used in the experiments. All the propellers had a diameter of 11 inches. Four APC Sport models (11  $\times$  4, 11  $\times$  6, 11  $\times$  8 and 11  $\times$  10) and three APC Thin Electric models (11  $\times$  7E, 11  $\times$  8E and 11  $\times$  10E), were chosen for the study. To be able to compare the noise generated between the sport and electric propeller models, both the sport and thin electric propeller models were tested for pitch 8 inches and 10 inches. Table 1 summarizes the characteristics of propellers tested in the present study. In addition to the pitch angle, the rotational speed of the motor was carefully adjusted from 2500 RPM to 5500 RPM with an incremental interval of 500 RPM.

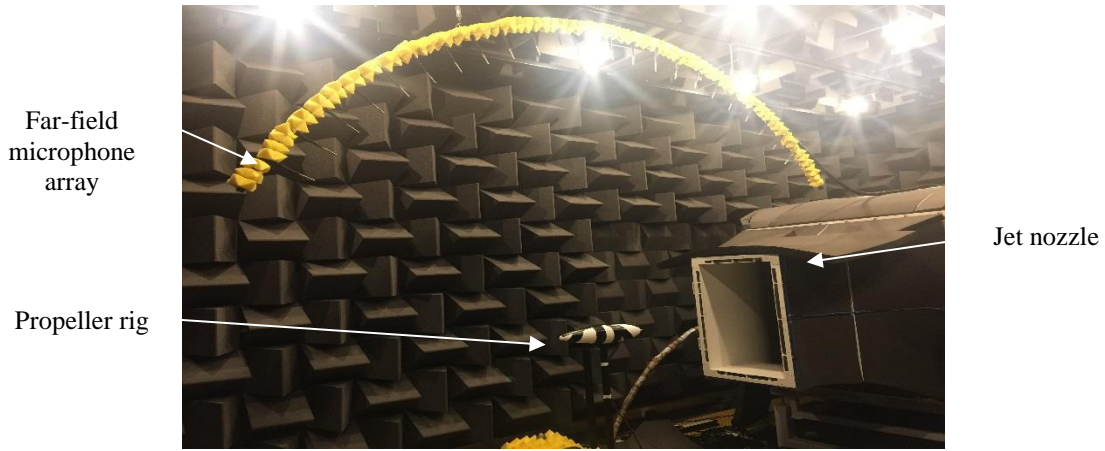


Figure 1. Experimental setup in the aeroacoustic tunnel.



(a) Physical map

(b) Structural map

Figure 2. Test rig design used for experiment.

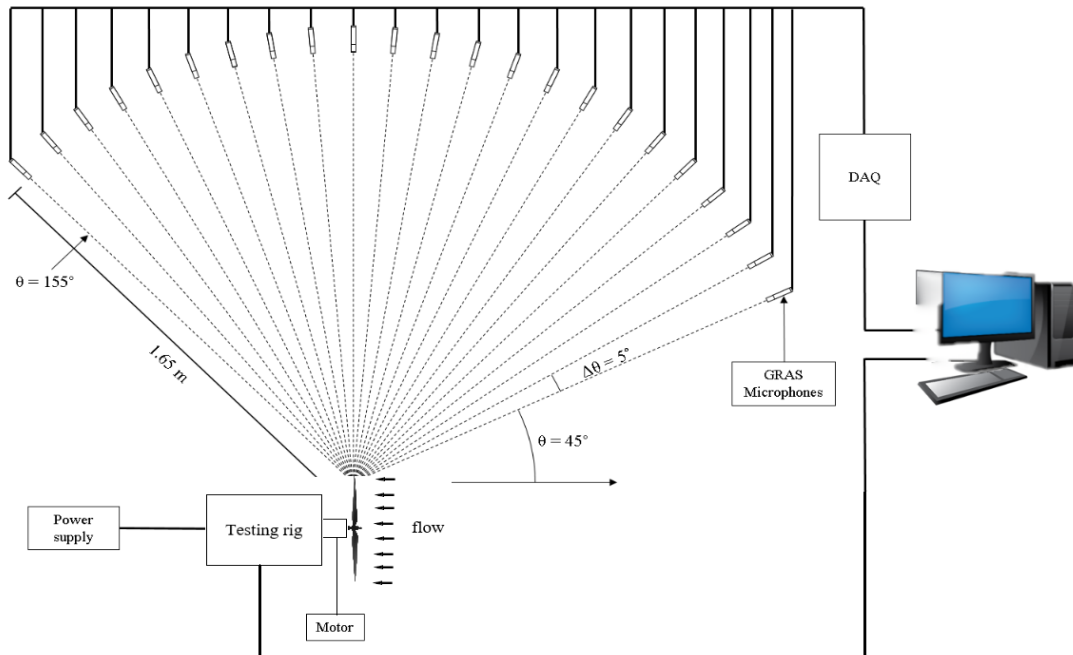









Figure 3. Schematic of the far-field directivity experiment.

Table 1. List and geometric details of the tested propellers.

Brand	Style	Designation Diameter/in×Pitch/in	Pitch angle $\beta$ at 75% radius/deg	Front view
APC	Sport	11×4	6.6	
APC	Sport	11×6	9.8	
APC	Sport	11×8	13.0	
APC	Sport	11×10	16.1	
APC	Thin Electric	11×7E	11.5	
APC	Thin Electric	11×8E	13.0	
APC	Thin Electric	11×10E	16.1	

### III. Results and Discussion

#### A. Aerodynamic performance

In this section, the effect of the flow velocity at different propeller rotational speeds is examined on the aerodynamic loads generated by different constant pitch propellers, as listed in Table 1. Measurements were performed at rotational speeds between 2500 and 5500 RPM, with an increment step of 500 RPM.

The main aerodynamic parameters of the APC 11×8 Sport propeller as a function of the inflow velocity ( $U$ ) are presented in Figure 4. Figures 4(a)-(d) compare the thrust (Figure 4(a) and 4(c)) and torque (Figure 4(b) and 4(d)) values obtained from experiments against the available APC thrust and torque data in the literature [20]. It is evident that measured data and available APC thrust and torque data are similar in magnitude and shows a similar trend with increasing the inflow velocity, that is, there are a slight decrease in the thrust and a slight increase in the torque from inflow velocity 0 m/s to 5 m/s, after which both the thrust and torque decrease continuously. Thrust decreases to zero, which is called wind-milling phenomenon. As expected, the highest rotational speed provides highest thrust and torque.

#### B. Effects of rotational speed

In this section, the effect of rotational speed on the acoustic signature is investigated. Figure 5 shows the far field noise powers spectral density, which is calculated via power spectral density (PSD) of the pressure fluctuations measured by the microphones. The PSD results of the pressure fluctuations of the APC 11×8 Sport propeller is presented at the flow velocities of  $U=0$  m/s, 5 m/s, 8 m/s, 12 m/s, 16 m/s and 20m/s, with different rotational speeds at  $\theta = 90$  degrees, see Figure 3.

Considering the case of the static thrust condition, where  $U=0$  m/s, the spectrum is dominated by the blade passing frequency (BPF), which is defined as the product of the number of blades and the rotational frequency, and its harmonics, as denoted by the sharp peaks spanning across the entire spectra, from approximately 30Hz to 1000Hz. The tonal noise contribution increases gradually as the rotational speed is raised, i.e. the tip speed increases. The tonal contribution at BPF for the 5500 RPM case is nearly 10dB higher than the noise level for the 2500 RPM case. Note that in a constant free-stream velocity, PSD increases with the increase in the blade rotational speed. For instance, PSD is always at 5500 RPM higher than that at 2500 RPM when the flow velocity is 12m/s. Moreover, the power spectral density PSD as a function of frequency shows discrete broadband noise, which increases with the increase of rotational speed, but only up to a maximum magnitude until 4000RPM.

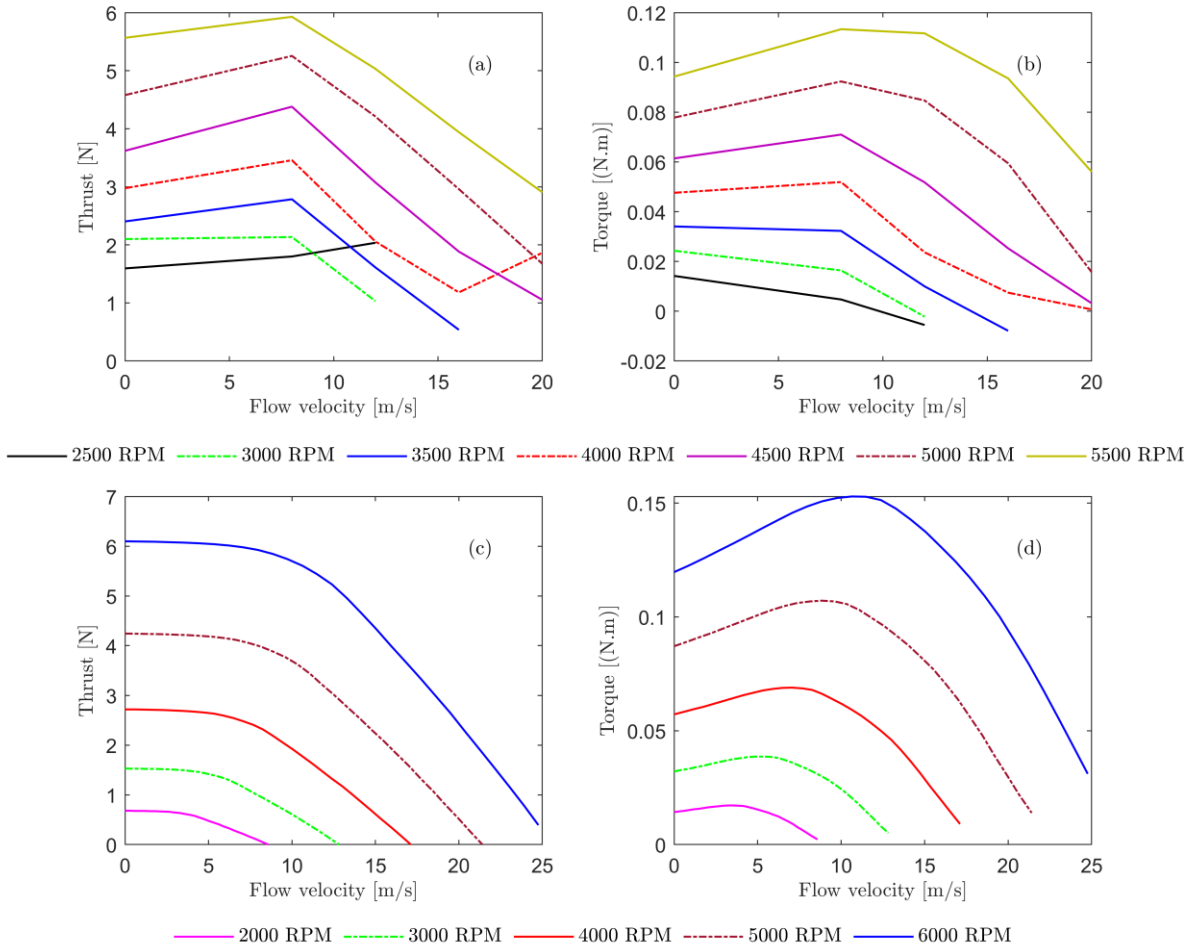


**Figure 4. Aerodynamic parameters (thrust and torque) as a function of flow velocity.**

(a) Measured thrust as a function of flow velocity;

(b) Measured torque as a function of flow velocity;

(c) APC thrust as a function of flow velocity;

(d) APC torque as a function of flow velocity.

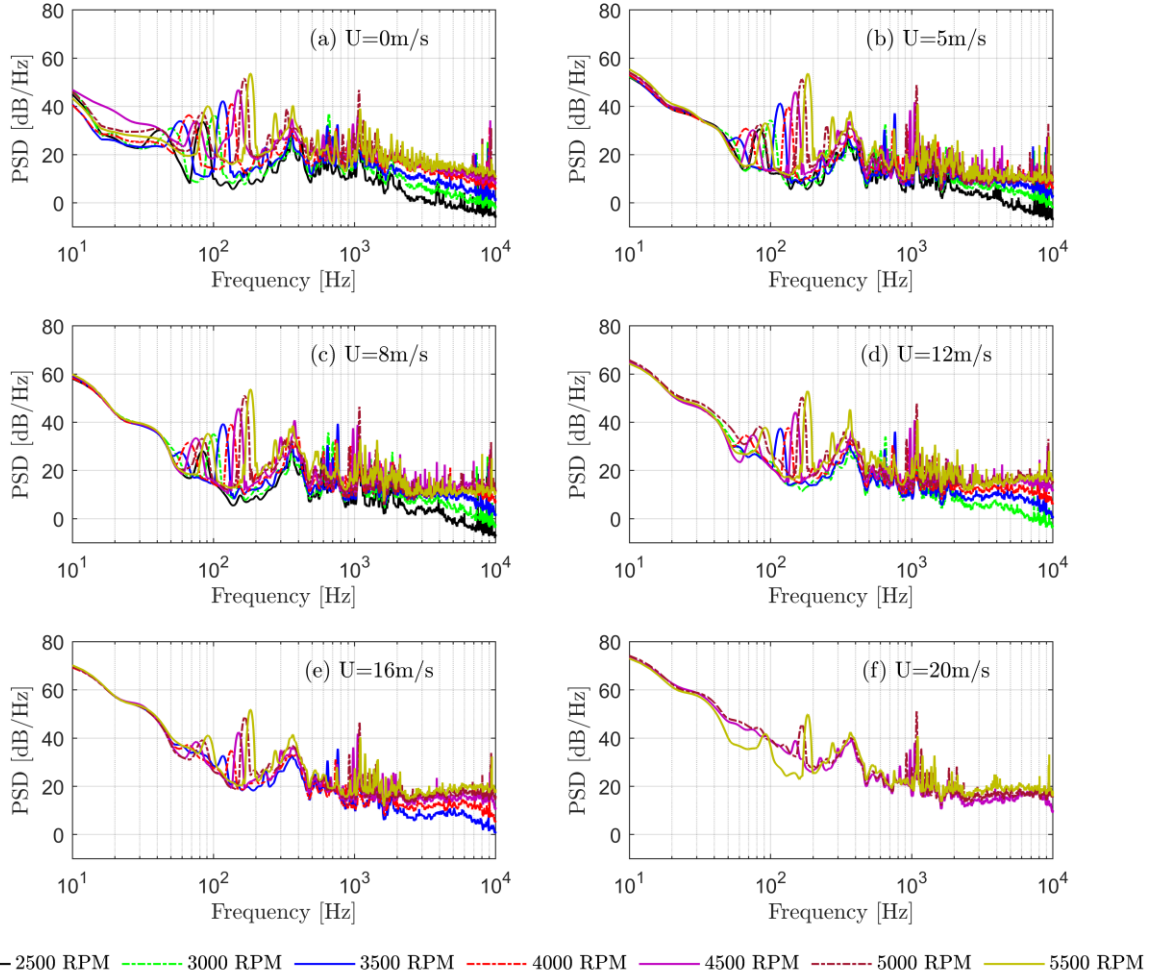


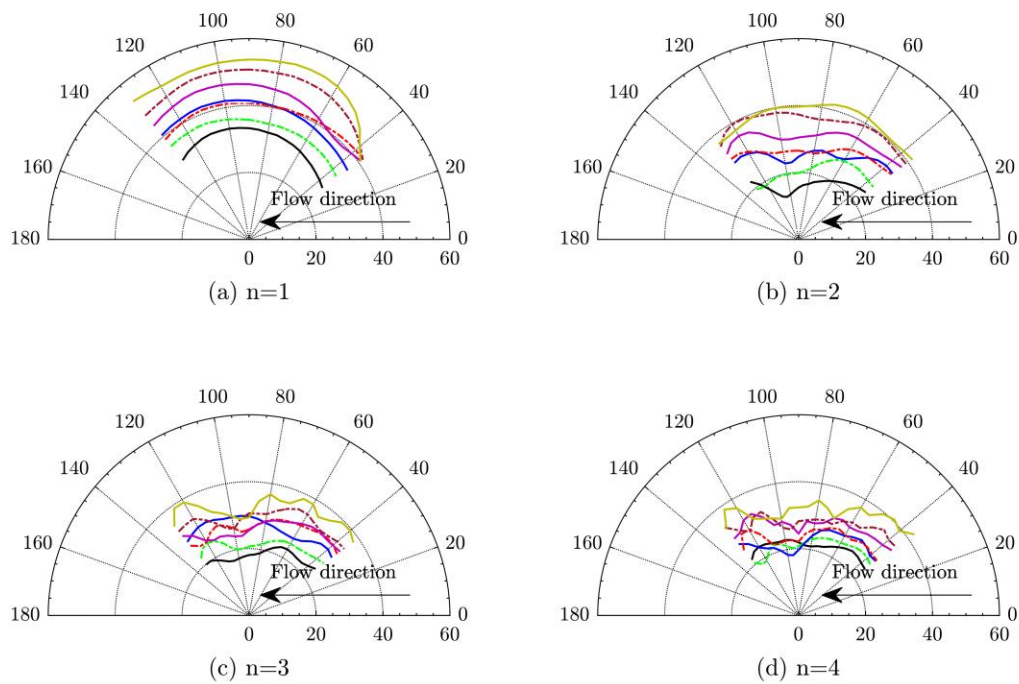
**Figure 5. PSD of APC 11×8 Sport propellers at six wind velocities at  $\theta = 90$  degrees to the plane of rotation.**

In order to better display the effects of flow velocity on SPL, the far-field directivity behavior is illustrated. Figures 6-8 are constructed to display the directivity behavior of tonal noise generated by propeller at flow velocities 0 m/s, 12 m/s and 20m/s, respectively. The rotational speeds were controlled between 2500 RPM and 5500 RPM with an increment of 500 RPM. Each figure has four separate graphs representing the results at BPF ( $n=1$ ) and its subsequent harmonics  $n=2, 3$  and 4. The calculated fundamental BPF and the first three harmonics for all rotational speeds are presented in Table 2.

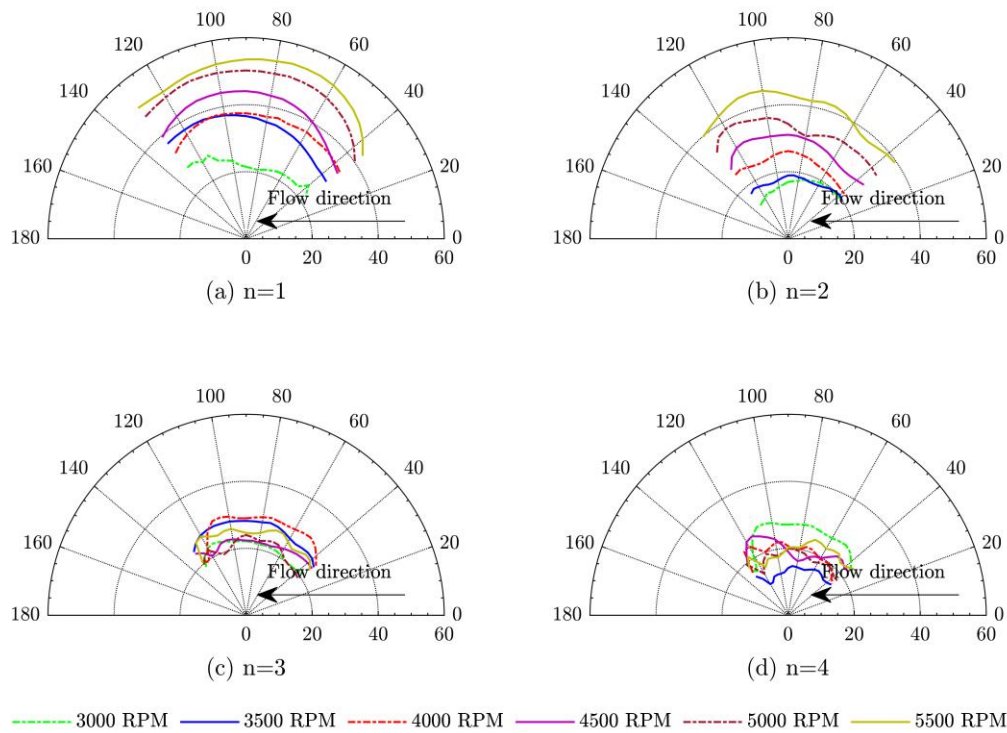
**Table 2. Fundamental blade passing frequencies and their first three harmonics at different rotational speeds.**

Rotational Frequency/Hz	1 <sup>st</sup> BPF/Hz	2 <sup>nd</sup> BPF/Hz	3 <sup>rd</sup> BPF/Hz	4 <sup>th</sup> BPF/Hz
41.7(2500RPM)	83.3	166.6	250.0	333.3
50(3000RPM)	100	200	300	400
58.3(3500RPM)	116.6	233.3	350	466.7
66.7(4000RPM)	133.3	266.7	400	533.3
75(4500RPM)	150	300	450	600
83.3(5000RPM)	166.7	333.3	500	666.7
91.7(5500RPM)	183.3	366.7	550	733.3





— 2500 RPM — 3000 RPM — 3500 RPM - - - 4000 RPM — 4500 RPM - - - 5000 RPM — 5500 RPM  
**Figure 6. Far-field directivity at the BPF and next three harmonics of APC 11×8 propellers at wind velocity 0m/s.**



— 3000 RPM — 3500 RPM - - - 4000 RPM — 4500 RPM - - - 5000 RPM — 5500 RPM  
**Figure 7. Far-field directivity at the BPF and next three harmonics of APC 11×8 propellers at wind velocity 12m/s.**

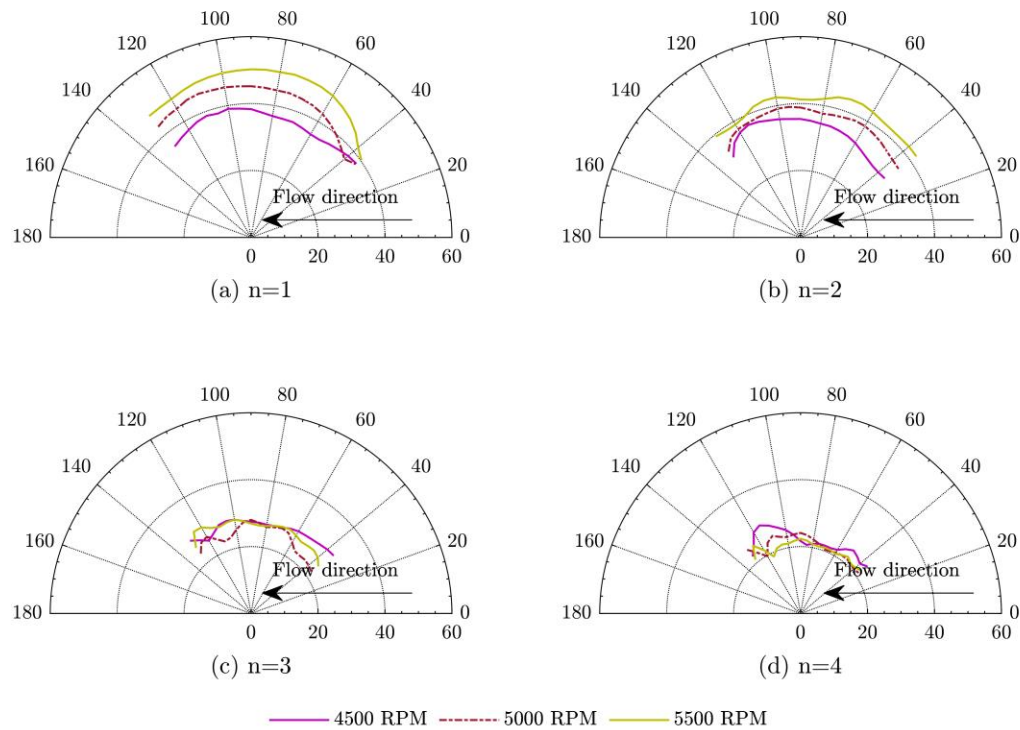


**Figure 8. Far-field directivity at the BPF and next three harmonics of APC 11×8 Sport propellers at wind velocity 20m/s.**

At the first blade passing frequency ( $n=1$ ) in Figures 6-8, the propeller noise seems to exhibit a cardioid behavior for most of the cases. The lower SPL values observed at lower polar angles, where the propeller is facing the flow. Nevertheless, in some of the cases, there is a slight deviation from the cardioid behavior as in the case of 4000 RPM. These deviations can possibly be attributed to the existence of a certain resonance on the experimental setup which alters the directivity. At higher blade passing frequencies ( $n=2, 3$  and  $4$ ), the directivity pattern transits from cardioid behavior to more complex directivity patterns. The complexity of the directivity pattern at the harmonics of the fundamental BPF attenuates with the introduction of free-stream velocity. Across all flow velocities, the lowest SPL has generally been observed to be between  $100^\circ \leq \theta \leq 120^\circ$  at all rotational speeds. The SPL was reduced at higher blade passing frequency ( $n=4$ ) with the increase of flow velocity (12m/s and 20m/s), as shown in figure 7(d) and figure 8(d).

### C. Effects of flow velocity

In this section, the effect of flow velocity on the noise generated by APC 11×8 Sport propeller is investigated. For each RPM, the free-stream velocity at which the propeller shifts to wind-milling state changes, hence the range of the flow velocity was varied for different rotational speeds appropriately. For instance, at 2500RPM, the propeller shifts to the wind-milling state at 8m/s, but at 3000 RPM, 3500 RMP and 4500RPM the propeller starts to perform at the wind-milling state at 12m/s, 16m/s and 20m/s, respectively. This wind-milling state means the propeller doesn't provide any thrust, as shown in figures 4 (a) and (c). For instance, propeller doesn't provide any thrust at inflow velocity  $U=12.8\text{m/s}$  and the motor's rotational speed  $\Omega=3000$  RPM, and at inflow velocity  $U=17.2\text{m/s}$  and the motor's rotational speed  $\Omega=4000$  RPM.

Figure 9 shows the PSD of the measured noise as a function of the rotational speed at varying flow velocity for rotational velocities of 3000 RPM, 4000 RPM and 5000RPM. To ease the interpretation, a close-up look for the region of interest is also presented for each RPM value on the right hand side of each plot. Comparing across Figures 9(a) to (c), a decrease in the tonal noise around the fundamental BPF with the increase of the flow velocity is observed for all RPM's. For instance, the tonal noise level associated with the BPF drops from

approximately 51dB to 46dB when the velocity increases from  $U=5$  m/s to 20 m/s at rotational speed of 5000RPM (i.e. Figure 9(c)). This may be due to the reduced aerodynamic loads with increased free-stream velocity. The broadband hump at 350Hz may be due to a combination of factors, such as the aerodynamic interactions between the shed vortices and experimental setup, as well as the resonance of some components in the test rig. A distinct behavior is observed, in the case of 3000 RPM, see figure 9(a), where the tonal noise around the BPF is completely disappears at  $U=12$  m/s. This can be associated to the fact that blades are not aerodynamically loaded at this speed.

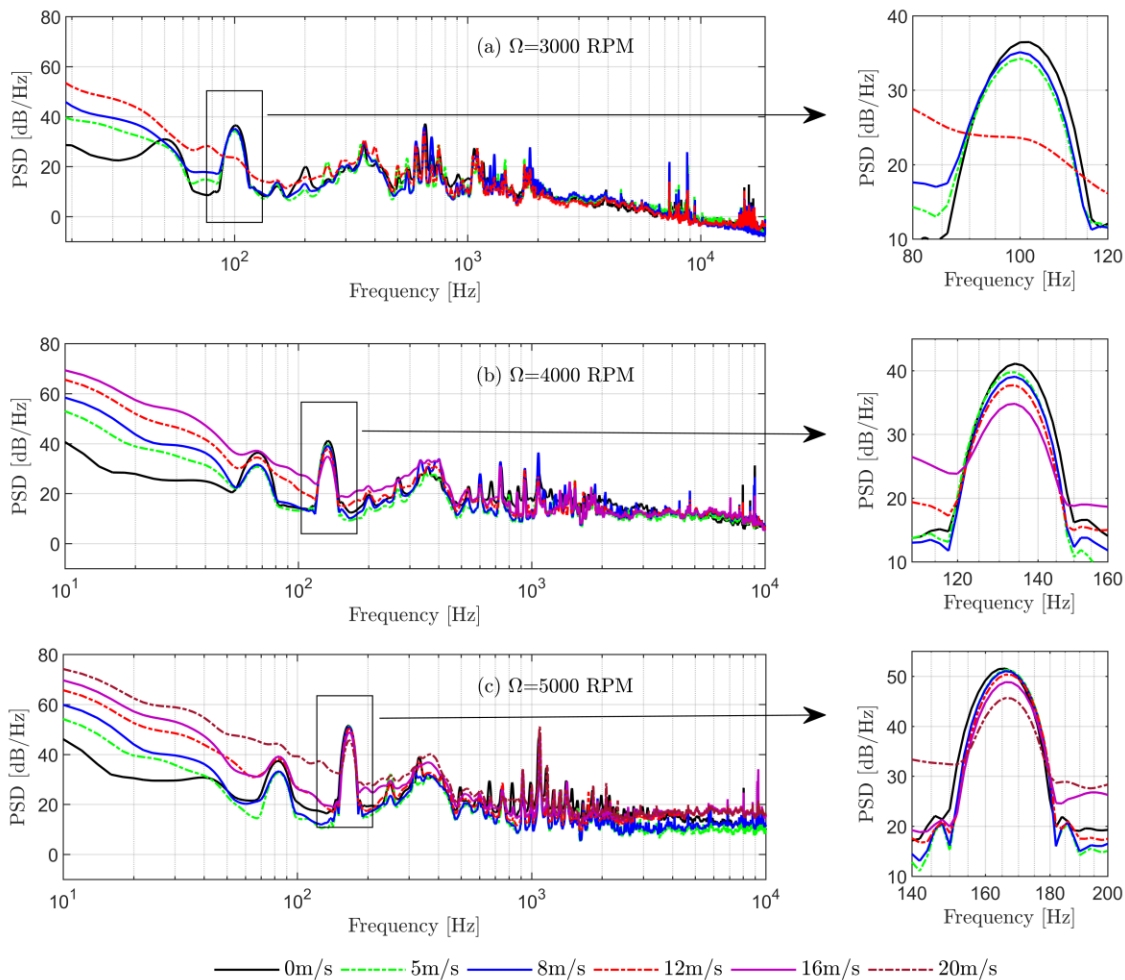


**Figure 9. PSD of APC 11x8 Sport propellers as a function of rotational speed at varying flow velocity.**

Figure 10 is presented to have a better insight on the effects of flow velocity and the resultant aerodynamic loads on the generated noise, The four graphs display the far-field noise power spectral density of the pressure fluctuations with respect to velocity, advanced ratio ( $J$ ), thrust and torque at 3000 RPM, 4000 RPM and 5000 RPM at BPF. Figure 10(a) and (b) indicates that increase in velocity or advanced ratio decreases the generated noise at 4000 RPM and 5000 RPM. For 3000 RPM the PSD level trend deviates from the gradual decrease at 8 m/s and corresponding advanced ratio. Considering Figure 10 (c) and (d), the PSD levels tend to increase with the aerodynamic loads, i.e. thrust and torque.

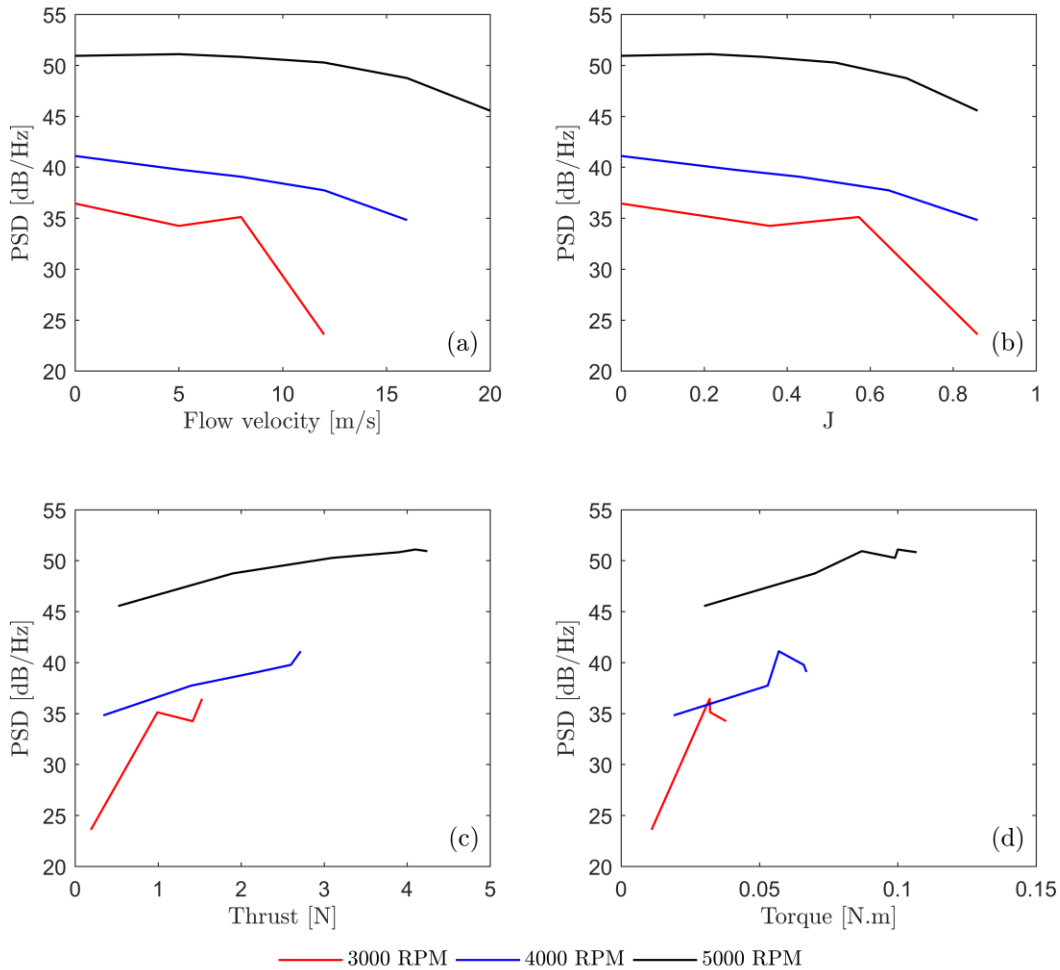


**Figure 10.** PSD of APC 11×8 Sport propellers as a function of (a) flow velocity (b) advanced ratio J (c) thrust and (d) torques at rotational speed of 3000 RPM, 4000 RPM and 5000 RPM at BPF.

#### D. Effects of pitch

At the given diameter of 11 inches, seven propellers with pitch angle of  $6.6 < \beta_{75\%R} < 16.1$  were used to measure the far-field noise power spectral density of the pressure fluctuations. Figure 11 displays PSD as a function of the free-stream flow velocity at varying rotational velocities at 3000 RPM, 4000 RPM and 5000 RPM at the first blade passing frequency. Considering all the graphs in Figure 10(a) to (c), the following results may be concluded. As the pitch angle increases the noise generated by the propeller increases. The PSD levels increase about 7dB from pitch 4 inches to 10 inches. Moreover, the thin electric propellers generate less noise compared to the sport propellers. Furthermore, as in line with the previous observations, the PSD levels increase with the increase in RPM, i.e. increase the effective speed of the blade tip.

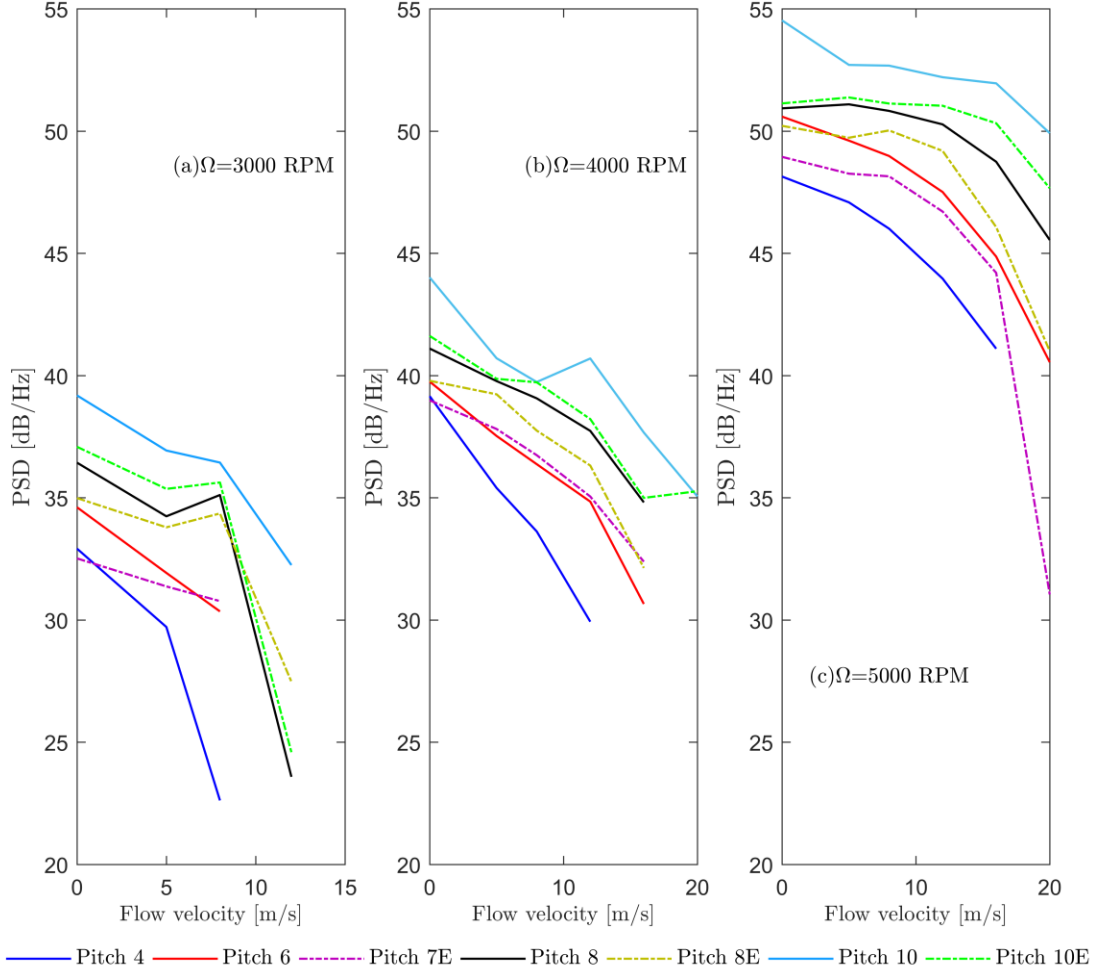


**Figure 11. PSD as a function of flow velocity at different rotational speeds for different pitch values at BPF.**

#### IV. Conclusion

This article described an experimental work to investigate the effect of propeller pitch and rotational speed on the noise generation by small diameter propellers (11 inches), in the forward-flow-flight condition with various flow velocities. To establish a link between aerodynamic and acoustic performances, the aeroacoustic noise levels and aerodynamic loads, were acquired simultaneously, thus allowing detailed analysis of far-field acoustic signatures as a function of shaft rotational speed and the corresponding aerodynamic loads (thrust and torque).

Results from acoustic measurement highlighted that the propeller noise signature consists of a series of discrete tones and broadband noise and that the spectra were dominated by the blade passing frequency and its harmonics regardless of the propellers used. The directivity study suggested that while the fundamental blade passing frequency exhibits cardioid behavior, its harmonics generate a more complex directivity pattern with lower power spectral density values. Furthermore, the power spectral density level increases with the increase in the rotational speed due to the increase the blade tip's speed. The experiments show that the aerodynamic loads and the level of generated noise is related. An increase in thrust and torque values tends to increase the PSD values. Moreover, it is shown that higher pitch values generate higher far-field noise power spectral density

at first blade passing frequency. Finally, the APC Sport propellers is shown to be noisier than APC Thin Electric propeller with the same pitch.

## References

- <sup>1</sup> Massey, K., Gaeta, R., "Noise Measurements of Tactical UAVs", 16th AIAA/CEAS Aeroacoustics Conference, Stockholm, Sweden, 2010.
- <sup>2</sup> Welch, Adrienne, "A cost-benefit analysis of Amazon Prime Air" (2015). Honors Theses. <https://scholar.utc.edu/honors-theses/47>
- <sup>3</sup> Blake, W. K., *Mechanics of Flow-Induced Sound and Vibration; Vol 2: Complex Flow-Structure Interactions*, Academic Press, London, 1986
- <sup>4</sup> Brooks, T. F., Pope, D. S. and Marcolini, M. A., Airfoil self-noise and prediction, NASA Reference publication No. 1218, Langley Research Centre, 1989
- <sup>5</sup> Miljković, D., Ivošević, J., Bucak, T., "Two vs. Three Blade Propeller – Cockpit Noise Comparison", 5<sup>th</sup> Congress of Alps-Adria Acoustics Association, Petrčane, Croatia, 2012
- <sup>6</sup> Bailey, J. E., "Mini-RPV Engine-Propeller Wind Tunnel Tests," National Free Flight Society Annual Symposium Proceedings, 1978.
- <sup>7</sup> Durand, W. F., "Experimental Research on Air Propellers," NACA Report 141, 1923.
- <sup>8</sup> Bass, R. M., "Small Scale Wind Tunnel Testing of Model Propellers," AIAA Paper 86–392, January 1986.
- <sup>9</sup> Asson, K. M. and Dunn, P. F., "Compact Dynamometer System That Can Accurately Determine Propeller Performance," *Journal of Aircraft*, Vol. 29, No. 1, 1992, pp. 8–9.
- <sup>10</sup> Brandt, J. B., Small-Scale Propeller Performance at Low Speeds, Master's thesis, Department of Aerospace Engineering, University of Illinois at Urbana-Champaign, Illinois, 2005.
- <sup>11</sup> Merchant, M. P., Propeller Performance Measurements for Low Reynolds Number Unmanned Aerial Vehicle Applications, Master's thesis, Department of Aerospace Engineering, Wichita State University, Kansas, 2005.
- <sup>12</sup> Merchant, M. P. and Miller, L. S., "Propeller Performance Measurements for Low Reynolds Number UAV Applications, AIAA Paper 2006–1127, January 2006.
- <sup>13</sup> Ol, M., Zeune, C., and Logan, M., "Analytical/Experimental Comparison for Small Electric Unmanned Air Vehicle Propellers," AIAA Paper 2008–7345, August 2008.
- <sup>14</sup> John, B. B., Michael, S. S., "Propeller Performance Data at Low Reynolds Number," AIAA Paper 2011–1255, January 2011.
- <sup>15</sup> Aleix C., Ethan P., Syamir A., "Investigation Towards a Better Understanding of Noise Generation from UAV Propellers," AIAA Paper 2018–3450, June 2018.
- <sup>16</sup> Nikolas S., Henry H., "Small Propeller and Rotor Testing Capabilities of the NASA Langley Low Speed Aeroacoustic Wind Tunnel," AIAA Paper 2017-3709, June 2017.
- <sup>17</sup> Mayer Yannick D., Kamliya Jawahar H., Szoke M. and Azarpeyvand M., "Design of an Aeroacoustic Wind Tunnel Facility at the University of Bristol", 2018 AIAA/CEAS Aeroacoustics Conference, AIAA 2018-3138, June 2018.
- <sup>18</sup> Liu, X., Kamliya Jawahar, H., Azarpeyvand, M., & Theunissen, R. (2017). Aerodynamic performance and wake development of airfoils with serrated trailing-edges. *AIAA Journal*, 55(11), 3669-3680.
- <sup>19</sup> Ali, SAS, Szoke, M, Azarpeyvand, M & Silva, CRId, 2018, "Turbulent Flow Interaction with Porous Surfaces". AIAA Paper 2018-2801, June 2018.
- <sup>20</sup> J.B. Brandt, R.W. Deters, G.K. Ananda, and M.S. Selig (insert date downloaded), UIUC Propeller Database, University of Illinois at Urbana-Champaign, retrieved from <http://m-selig.ae.illinois.edu/props/propDB.html>.